Heliyon xxx (xxxx) xxx

Contents lists available at ScienceDirect

Heliyon

journal homepage: www.heliyon.com

Heliyon

Kinetic, isotherm and mechanism investigations of the removal of phenols from water by raw and calcined clays

Hassan Ouallal [a,b], Younes Dehmani [c], Hamou Moussout [c,*], Lahcen Messaoudi [b], Mohamed Azrour [a]

[a] Laboratory of Physic-chemistry Materials, Department of Chemistry Fundamental and Applied, Faculty of Sciences and Techniques, Moulay Ismaïl University, PB 509, Errachidia, Morocco

[b] Materials, Membranes and Processes of Separation, Department of Chemistry, Faculty of Sciences, Moulay Ismaïl University, PB 11201, Zitoune, Meknes, Morocco

[c] Laboratory of Chemistry, Biology Applied to the Environment, Faculty of Sciences, Moulay Ismaïl University, PB 11201-Zitoune, Meknes, 50060, Morocco

ARTICLE INFO

Keywords:
Chemical engineering
Environmental science
Physical chemistry
Inorganic chemistry
Materials chemistry

ABSTRACT

In this work, the phenols removal of phenol from water by raw clay (RCG) and calcined one at 1000 °C (CCG) of Goulmima city (Morocco) was investigated. The kinetics and isotherms experiments were also studied at pH = 4. The results indicated that the phenol adsorption reached equilibrium within 3 h, and the removal of phenol was enhanced at the same temperature by CCG (2.932 mg/g) adsorbent, compared to RCG (1.640 mg/g) due to the removal of organic matter by heat treatment, and an increase in adsorption temperature, indicating the endothermic process. The adsorbents were characterized by means of X-ray fluorescence, FTIR, XRD, B.E.T, and TGA/DTA analysis and showed that the clay consists essentially of silica and alumina. The experimental data were examined by using linear and nonlinear forms of the kinetics and the isotherms models. Based on the errors of the calculated values of R^2 (Coefficient of determination), χ^2 (Chi-square) and standard deviation (Δq (%)), it was found that the nonlinear forms of second-order kinetic model and Freundlich and Redlich-Peterson (R–P) isotherm models are best fit the experimental data for both adsorbents. However, the enthalpy ΔH° is less than 20 kJ/mol and the free energy ΔG° has a negative value, which shows that the adsorption is done physically and spontaneously on heterogeneous sites. The interest of this study is the use of FTIR and XRD to determine the effect of calcination on the phenol adsorption mechanism. However, the analysis of both adsorbents, before and after adsorption of phenol, shows that the adsorption mechanism of phenol is provided by the hydrogen bonding of the water molecules.

1. Introduction

Natural water resources are becoming increasingly scarce; thus, the state of the environment has become one of the major concerns of humanity because of its degradation. This degradation is mainly due to the industrial development that generates discharged effluents into the receiving environment without any treatment in most cases. These releases consist of toxic elements and/or chemical compounds, which pose a serious threat to our environment due to their abundant presence in liquid and gaseous forms. Pollutants that alter the quality of water include phenolic compounds. Indeed, these products are widely used as pesticides, explosives, dyes and as solvents and precursors in the chemical industry. Currently they are of great concern since of their toxicity to ecosystems and their adverse effects on human health. Phenols are found in wastewater, as well as in all-natural water systems [1] and are considered as one of the pollutants priority because of their unpleasant tastes, odors and toxicity [2, 3], even at low concentrations.

However, the removal of phenolic compounds from water is difficult because of their high stability and solubility [4] and the development of effective methods to remove phenolic compounds from water is an important topic.

Many methods have been developed for the treatment of phenol polluted water. These methods can be divided into three broad categories: physical, chemical and biological. The most frequently used techniques are: solvent extraction [5], adsorption [6], filtration [7], precipitation [8], coagulation [7], and ion exchange [9]. Due to the high abundance of (natural) adsorbent, the methods based on adsorption reaction are the most investigated and adopted [10, 11]. Activated carbons

* Corresponding author.
E-mail address: moussouthammou@gmail.com (H. Moussout).

https://doi.org/10.1016/j.heliyon.2019.e01616
Received 6 March 2019; Received in revised form 29 March 2019; Accepted 29 April 2019
2405-8440/© 2019 Published by Elsevier Ltd. This is an open access article under the CC BY-NC-ND license (http://creativecommons.org/licenses/by-nc-nd/4.0/).

Please cite this article as: H. Ouallal et al., Kinetic, isotherm and mechanism investigations of the removal of phenols from water by raw and calcined clays, Heliyon, https://doi.org/10.1016/j.heliyon.2019.e01616

are undoubtedly among the most used non-natural materials [12, 13, 14], but they have numerous drawbacks including, for example: the cost of regeneration, the intra particulate resistance in the adsorption process and the low mechanical resistance [15]. As a result, the use of natural inorganic materials as adsorbents has become a more targeted field of research [16, 17, 18], and among the most commonly used inorganic materials there are clays and clay minerals [19].

Properties of clays depend strictly on the crystal chemical feature of the clay minerals of which they are composed. However, due to their cation exchange capacity, low cost, and high availability clays were often considered to study the interaction mechanisms with various organic and inorganic pollutants [20, 21, 22, 23, 24, 25, 26, 27, 28, 29, 30, 31].

The aim of this study is the valorization of a raw Moroccan clay (RCG: raw clay from Goulmima) and calcined one at 1000 °C (CCG: calcined clay from Goulmima), in the retention of phenol from aqueous solution using batch adsorption experiments. Before their use, the adsorbents were characterized by X-ray fluorescence, FTIR, XRD, TGA/DTA and B.E.T. For better prediction of kinetic and isothermal experimental data of phenol adsorption onto RCG and CCG, the linear and non-linear forms of the different kinetic and isothermal models were used and compared to get the corresponding parameters. The coefficient of determination R^2, the standard deviation (Δq (%)) and the chi-square (χ^2) of the tests were calculated to discover the validity of the different forms of these models. The mechanism study was also evaluated based on the adsorption isotherms as well as on the adsorbent analysis after phenol adsorption by FTIR and XRD.

2. Experimental

2.1. Raw material

The used clay in this work is taken from the south of Atlas of Morocco (Goulmima). This clay is crushed and sieved using sieves of known opening. Only the particle size less than 315 μm is retained and a portion of this clay was calcined at 1000 °C according to the thermal program as follow:

(T = 25 °C, 2°/min) → (T = 100 °C, 2°/min) → (T = 250 °C, 4°/min) → (T_f = 1000 °C, 2°/min, t = 3 h)

2.2. Point of zero charge

The pH of the point of zero charge (pH_{pzc}) of the clay is determined according to the following procedure: in each 10 beakers, we put 20 mL of NaCl (0.01M). The pH of these latter solutions is adjusted by adding NaOH (0.1M) or HCl (0.1M) to prepare solutions with initial pH_i values between 1 and 14. After fixing the initial pH_i, 20 mg of the clay is added to each solution and stirred for 24 h at room temperature, and then the final pH_f is measured to plot the $pH_f = f(pH_i)$ curve. The pH_{pzc} is determined at$pH_f = pH_i$ [32].

2.3. Characterizations of samples

Firstly, the X-rays fluorescence was carried out using an "Axion" type of X-ray fluorescence spectrometer, with dispersion of 1 kW wavelength. This type of chemical analysis was carried out at the UATRS laboratory and CNRST in Rabat, Morocco. Next, X-ray diffraction (XRD) patterns were recorded using an X'PERT MPD-PRO wide angle X-ray powder diffractometer provided with a diffracted beam monochromator and Ni filtered CuKα radiation (λ = 1.5406 Å). The value of 2θ angle was scanned between 4° and 30° range with a counting time of 2.0 s at steps of 0.02°. Then, Fourier transform infrared (FTIR) of RCG and CCG were characterized by using a Fourier transform infrared spectrometer (VERTEX70). The samples were prepared in KBr discs in the usual way from very well dried mixtures of about 4% (w/w). FTIR spectra were recorded from 4000 to 400 cm^{-1}. ThermoGravimetric Analysis/Differential Thermal Analysis (TGA/DTA) analyses were carried out in air atmosphere using LABSYS/evo thermal. The samples were linearly heated ($T = T_0 + \beta . t$) from ambient to 900 °C at a heating rate of 20 °C/min. Finally, BET Nitrogen adsorption measurements were obtained using a Micromeritics ASAP 2010 to obtain the textural parameters.

2.4. Batch adsorption experiments

The adsorption experiments were carried out at constant temperatures (T = 20, 40 and 60 °C) at pH = 4. Under stirring at 600 rpm for an adsorption time, a solution of phenol (20 mL of initial concentration C_i varied between 10 and 50 mg/l) was brought into contact with a mass of 0.2 g of the adsorbents. In the end of the reaction, the mixtures are filtered and analyzed by UV/Visible. The residual concentration Ce is determined from a calibration curve of the UV/Visible spectrometer (Shimadzu, UV-1240) at λ = 270 nm. The following equation is used to determine the amount adsorbed:

$$Q_{ads} = \frac{C_0 - C_e}{m_{adsorbent}} \times V_{sol} \quad (1)$$

Q_{ads}: is the adsorption capacity (mg/g), C_0: is the initial concentration of phenol (mg/L), C_e: residual Concentration of phenol (mg/L), m: presents mass of adsorbent used (g) and V_{sol}: mains the volume of the solution of phenol (L).

2.5. Kinetic and isothermal modelling

In order to determine the adsorption mechanism of phenol adsorption on both solids (RCG and CCG), the experimental data were adjusted using linear and nonlinear models respectively. Indeed, the modelling of the adsorption kinetics was carried out by the pseudo-first order, pseudo-second order and Weber-Morris intra-particle models:

$$q_t = q_e\left(1 - e^{-k_1 t}\right) \quad (2)$$

$$q_e = \frac{q_e^2 k_2 t}{q_e k_2 t + 1} \quad (3)$$

$$q_t = k_{id}\sqrt{t} + C_i \quad (4)$$

While those of the isotherms were carried by the Langmuir, Freundlich and Redlich-Peterson models:

$$\text{Langmuir} \quad q_e = \frac{q_m K_L C_e}{1 + K_L C_e} \quad (5)$$

$$\text{Freundlich} \quad q_e = K_F C_e^{1/n} \quad (6)$$

$$\text{Redlich} - \text{Peterson} \quad q_e = \frac{A C_e}{1 + K(C_e)^{\beta}} \quad (7)$$

With $A = K_R q_m$

The validity of these models was confirmed by error analysis calculations, such as the coefficient of determination (R^2), the standard deviation (Δq (%)) and the chi-square analysis (χ^2):

$$\Delta q(\%) = 100 \times \left\{ \frac{\sum_{i=1}^{n} \left[\left(q_{\exp} - q_{cal}\right)/q_{\exp} \right]^2}{n-1} \right\}^{1/2} \quad (8)$$

$$\chi^2 = \sum_{i=1}^{n} \frac{\left(q_{\exp} - q_{cal}\right)^2}{q_{\text{cal}}} \quad (9)$$

Withq$_m$: is the adsorption capacity at equilibrium (mg.g^{-1}); C$_e$ (mg.L^{-1}): is the residual concentration at equilibrium, and K$_L$ (L·mg^{-1}) represents the ratio of the rate constant of adsorption and desorption. . k$_d$ and C are the rate constant of intraparticule diffusion and the thickness of layer, respectively. K$_F$ and n are Freundlich constants that express the capacity and the adsorption intensity, respectively. K et β (0 <β < 1) are the R–P constants.

3. Results and discussion

3.1. Physico-chemical analyzes of clays (adsorbents)

3.1.1. X-rays fluorescence

The results of these analyzes show that the studied RCG consists essentially of silica (34.1%), alumina (10.5%) and calcium (22.1%). While, CCG is composed of silica (54.1%) and alumina (26.2%). The calcination decreases the calcium content and increases that of silica and alumina. In addition, the alkaline and alkaline-earth metal oxide contents are low (Table 1), these chemicals analyze show that the alumina content 10.5% is low compared to the alumina of the refractory clays: 45% [33]. This low content of alumina is entrusted to ceramic products and the presence of calcite reduces the sintering shrinkage. The increases of silica and alumina contents are explained by the transformation of kaolinite into mullite ($3Al_2O_3$, $2SiO_2$).

3.1.2. FTIR

Fig. 1 shows the FTIR spectra of RCG and CCG. Indeed, the spectrum recorded for RCG has a broad absorption band around 3425 cm^{-1} due to the stretching and flexing vibrations respectively of H_2O adsorbed on the surface and between the layers of the clay [34, 35, 36]. The 3650 cm^{-1} band can be attributed to the stretching vibration of the hydroxyl group in different environments (Al, AlOH), (Al, MgOH) or (Al, FeOH) [37, 38]. The bands observed at 2870, 1800, 1435, 870 and 715 cm^{-1} are attributed to the deformation and elongation vibration of the Calcite ($CaCO_3$) [39]. While, the band appeared at 800 cm^{-1} is assigned to the vibration deformation of the Si–O–Al bond. The 1030 cm^{-1} band corresponds to the elongation vibration of Si–O–Si bond in kaolinite or Quartz, and the 470 and 520 cm^{-1} bands are attributed to the deformation vibrations of Si–O bond in quartz [40, 41]. However, in the CCG spectrum, the appearance of the new bands, namely the 900 cm^{-1} band, corresponds to the bending vibration of the Al–O and Si–O bonds in the Mullite [42] and the band appeared at 645 cm^{-1} corresponds to the bending vibration of the Fe–O bond in Hematite. The comparison of the two FTIR spectra, of RCG and CCG, indicate that the calcination affects the band at 3425 cm^{-1} of water and reveals the bands of Mullite and Hematite that did not appear in the initial spectrum.

3.1.3. XRD

Fig. 2 presents the diffractograms of RCG (a) and CCG (b). the diffractogram (a) indicates that RCG consists essentially of Qaurtz (Q), Kaolinite (K) and Illite (I). however, the CCG diffractogram shows the disappearance of the phases and the appearance of new mineral phases namely; Mullite (m) and calcium silico-aluminate (csa) [43] and also the transformation of a part of quartz (β) in cristobaliteβ (cb) then in tridymite γ (t) [39]. The obtained results, using both XRD and FTIR indicate the transformation of kaolinite into Mullite. These result are in agreement with reference [44].

3.1.4. TGA/DTA

The TGA curves (Fig. 3) show a high thermal stability of RCG (Fig. 3a) and CCG (Fig. 3b) up to 800 °C because it is just the loss of mass attributed to water adsorbed in the surface. Indeed, the DTG thermogram of RCG indicates the presence of two endothermic peaks, the first peak that appeared at 120 °C corresponds to the dehydration accompanied by the loss of mass (1.29%) of the physiosorbed water, the second peak that appeared at 656 °C corresponds to dihydroxylation, it is the reaction in which the hydroxyls are removed from kaolinite and illite and the metakaolinite is formed [35]. The decomposition temperature depends on the origin of the material, the experimental conditions, the partial pressure of water vapor, and the maintenance of a partial pressure of water vapor influences the dihydroxylation [34]. In addition, the thermogram of CCG has more of surface-adsorbed water, two endothermic peaks, the first at 780 °C is attributed to decarbonation and the second at 892 °C corresponds to recrystallization. Indeed, the metakaolinite undergoes a structural rearrangement: it is transformed into mullite: $3Al_2O_3$ and $2SiO_2$ which is in agreement with the obtained results on the spectroscopy FTIR and XRD.

3.1.5. B.E.T

The Fig. 4 present the nitrogen adsorption/desorption isotherms and pore size distribution at 77 K of RCG (Fig. 4a) and CCG (Fig. 4b). It is observed that the obtained isotherms are the type IV, according to the IUPAC classification, characteristic of mesoporous solids [45, 46, 47]. H3 type hysteresis is a characteristic of porous solids whose size, distribution and pore shape are not uniform. The specific surface area (Table 2) obtained by the B.E.T method [48] is 25.35 m^2/g and 62.20 m^2/g for RCG and CCG, respectively. The distribution of the pore diameters (Fig. 4a and 4b inserted) is obtained using the BJH method based on a discrete analysis of the desorption branch of the isotherm. It is seen that the pore diameters are 38.36 Å and 53.25 Å for RCG and CCG, respectively, indicating a mesoporous structure [48].

3.2. Point of zero charge of both sample

The pH$_{pzc}$ is an important parameter in adsorption process, since it gives the information about the surface charge of adsorbents [6]. Fig. 5 shows the pH$_{pzc}$ of RCG (a) and CCG (b). The curves represent the variation of pH$_f$versus pH$_i$ for both solid. The pH$_{pzc}$ of RCG and CCG are 7.84 and 8.58, respectively. Thus, for higher value of pH, the surface is negatively charged. While for pH below 8.58 and 7.84 the surface is positively charged. The adsorption of phenol is more important in the case of surfaces with positive charges, for this we worked in pH < pH$_{pcn}$ [32] for the phenol adsorption onto RCG and CCG.

3.3. pH effect

The adsorption capacity of phenol decreases as increasing slightly the pH. Indeed, the equilibrium adsorption capacities are 2.88 mg. g^{-1} and 2.54 for pH = 4 and 11, respectively. This could be explained by the fact that in the basic state (pH > pH$_{pcn}$), the dominant charge of the surface of the adsorbents are negative, which decreases the adsorption of phenolates carrying the same charge. In the acidic state, the positive charges are dominant at the surface of the adsorbent and so there is a substantially high electrostatic attraction between the positive charges of the surface of the adsorbent and the negative charges of the formed phenolates which promote the adsorption [32]. Indeed, the value of pH is fixed at 4 for adsorption process giving to the fact that, for pH > 9 the phenol

Table 1
Chemical composition of RCG and CCG.

Oxides		SiO_2	Al_2O_3	CaO	MgO	Fe_2O_3	K_2O	Na_2O	TiO_2	LOI
(% mass)	RCG	34.1	10.5	22.1	2.6	3.03	1.51	0.454	0.443	24.8
	CCG	54.15	26.23	1.25	2.00	1.90	0.70	3.08	1.39	9.30

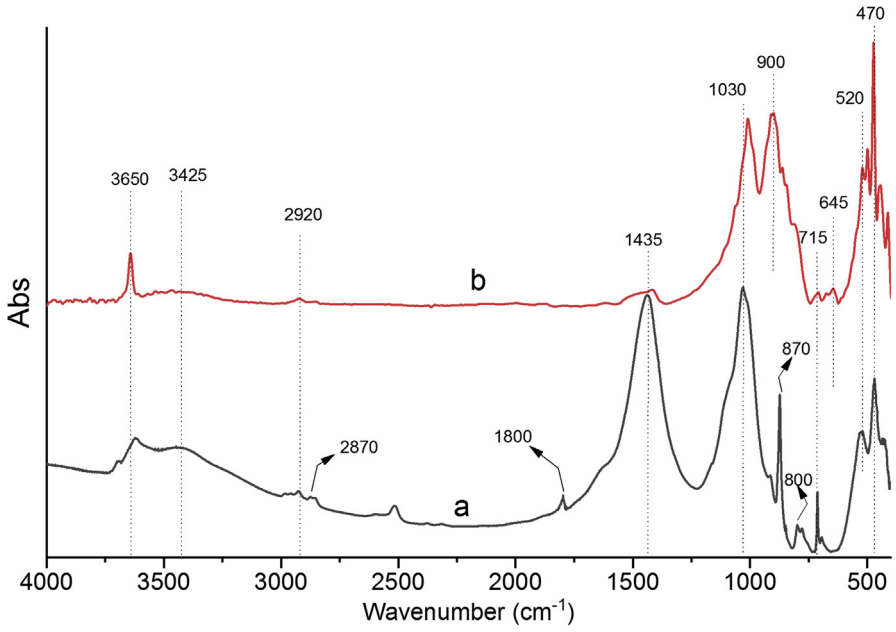

Fig. 1. FTIR spectra of RCG (a) and CCG (b).

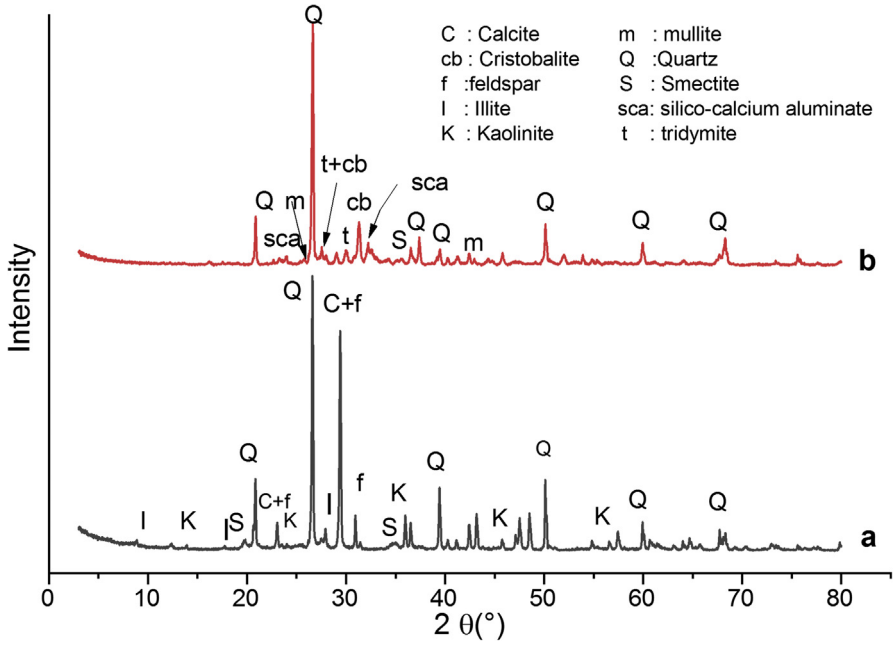

Fig. 2. XRD patterns of RCG (a) and CCG (b).

exists in the form of phenolates $C_6H_5O^-$ (pKA = 9.95) and in molecular form at acid state [49].

3.4. Adsorption kinetics

The adsorption kinetics of phenol onto RCG and CCG at different temperatures, with nonlinear models of pseudo-first order and pseudo-second order, are shown in Fig. 6 below. The adsorption is very fast during a contact time which does not exceed 4 h for all temperatures, the adsorption quantities for RCG at T = 20, 40 and 60°C are 1.03, 1.11 and 1.63 mg/g, and for GCC are 1.51, 1.83 and 2.93 mg/g, respectively. It is noted that the increase in temperature increases the adsorbed quantity, which can be explained by the promotion of the diffusion of the molecules through the outer boundary layer and the internal pores of the particles of the adsorbent, probably following the decrease of the viscosity of the solution. This increase with temperature indicates that the adsorption process is controlled by an endothermic reaction [50]. We find that the amount adsorbed by CCG is high compared to that of RCG, indicating that calcination eliminates the organic matter which competes with phenol, this is confirmed by the increase of the specific surface (B.E.T. result).

To elucidate the adsorption kinetics and mechanism of phenol onto both adsorbents, the experimental points were analysed using linear and non-linear kinetic models of pseudo-first order and pseudo-second order. To identify the most suitable model, the experimental data were analysed using the calculations R^2, χ^2 and Δq (Table 3). Thus, the kinetic parameters can be determined for such a model by plotting the linear and non-linear forms of the equations above. Fig. 6 represents the nonlinear

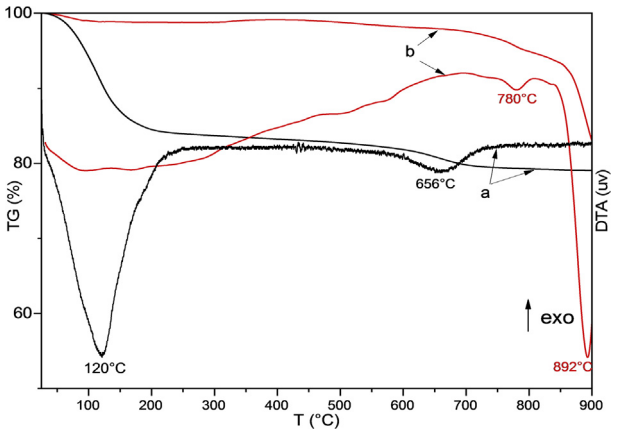

Fig. 3. TGA/DTA thermograms of RCG (a) and CCG (b).

curves of the two pseudo first-order and pseudo-second order models (the straight lines of the linear models are not presented), while the values deduced from different kinetic parameters are given in Table 3. According to these parameters, we find that the model of pseudo second order (linear and non-linear forms) describes well the experimental points for the three adsorption temperatures. The q_{cal} values are practically in agreement with those found experimentally (q_{exp}) (Table 3). In addition, the found values for the rate constants k_2 of the pseudo-second order model increase from 20 °C to 40 °C. Moreover, this result was confirmed by the values of the coefficient of determination, R^2 very close to 1, and by the calculated values of χ^2 and Δq.

Recently, several criticisms have been made about the application of linear kinetic models [51, 52] due to differences in the error function that varied during the linearization of the nonlinear equation, because they led to the erroneous values of the kinetic parameters intrinsic.

The Weber-Morris intra-particle model was tested by plotting q_t versus $t^{0.5}$ to study the phenol diffusion process of the solution to the external and internal surface of RCG and CCG. Fig. 7 shows the graphs, from this model for both adsorbents, it is found that the adsorption of phenol goes through two stages for the two solids. The second stage corresponds to a state of equilibrium where there is no more evolution of the adsorption capacity. According to this model, if only intra-particle scattering is involved in the process, the line passes through the origin, which is not the case in this study (Table 4) implying that intra-particle scattering is not the only one that controls the rate of adsorption of phenol onto both adsorbents.

The activation energies can be calculated from the pseudo-second order rate constant (k2) using the Arrhenius equation:

$$Ln(k_2) = Ln(A) - \frac{E_a}{RT} \quad (10)$$

Where k_2 is the pseudo-second order rate constant (g/mg.min), A the pre-exponential factor (min^{-1}), R is the gas constant (8.314 J/mol.K), T the adsorption temperature (K) and Ea is the apparent activation energy of

Table 2
Textural characteristics of RCG and CCG.

	B.E.T		
	Specific surface (m^2/g)	Volume (cm^3/g)	Diameter (Å)
RCG	25.351	0.034	38.36
CCG	62.205	0.094	53.25

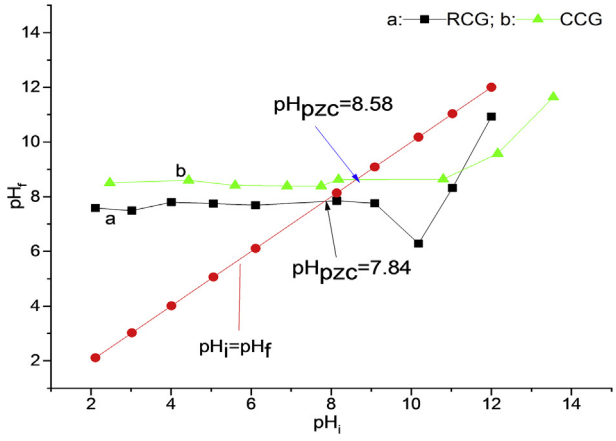

Fig. 5. pH_{pzc} of RCG (a) and CCG(b).

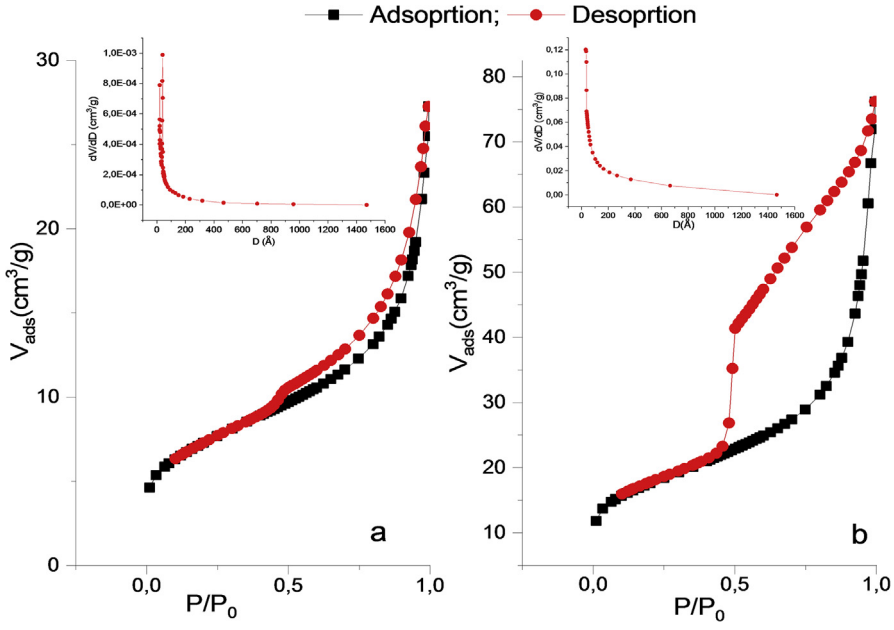

Fig. 4. N_2 adsorption/desorption isotherms of RCG (a) and CCG (b).

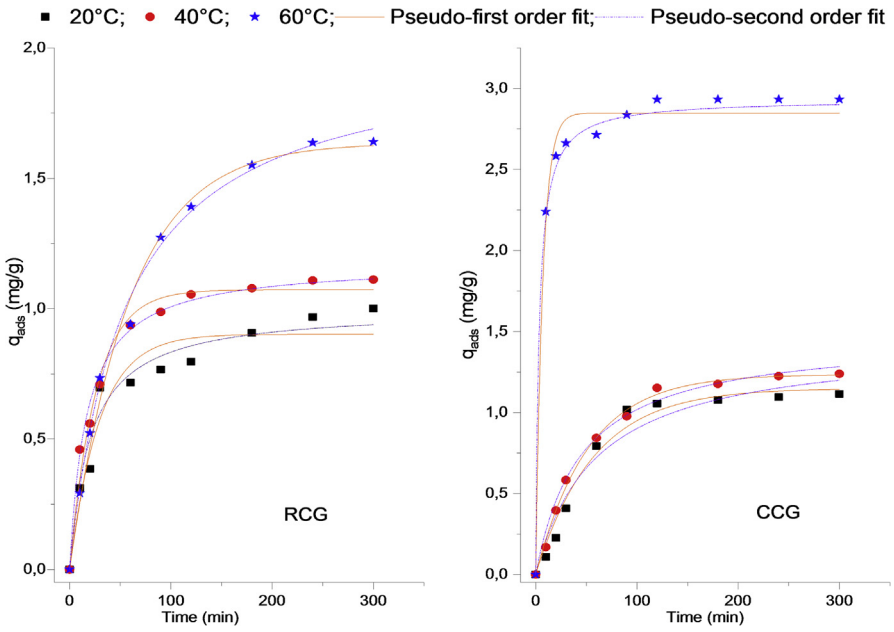

Fig. 6. Adsorption kinetics with nonlinear models of pseudo-first order and pseudo-second order of phenol (C_0 = 30 mg/l) onto RCG and CCG at pH = 4.

Table 3
Kinetic parameters of linear and nonlinear modeling of phenol adsorption at different temperatures onto RCG and CCG.

	Sample	RCG						CCG					
		Linear equations			Nonlinear equations			Linear equations			Nonlinear equations		
Models	q_{exp} (mg/g)	1.001	1.112	1.640	1.001	1.112	1.640	1.115	1.239	2.932	1.115	1.239	2.932
	T (°C)	20	40	60	20	40	60	20	40	60	20	40	60
LPFO	q_e (mg/g)	8.479	8.346	8.397	0.902	1.073	1.635	8.554	8.486	6.791	1.149	1.235	2.849
	k_1 (min^{-1})	3.083E-04	3.300E-04	6.391E-04	0.034	0.388	0.017	4.385E-04	4.637E-04	6.446E-04	0.017	0.019	0.143
	Δq (%)	1.011	1.014	1.016	0.041	0.024	0.037	1.015	1.014	1.052	0.047	0.019	0.039
	χ^2	0.004	0.007	0.010	0.007	0.003	0.003	0.008	0.008	9534.000	0.005	0.001	0.010
	R_1^2	0.685	0.595	0.800	0.940	0.983	0.992	0.690	0.734	0.297	0.978	0.996	0.988
LPSO	q_e (mg/g)	1.082	1.164	1.982	1.002	1.177	1.997	1.519	1.506	2.974	1.437	1.475	2.932
	k_2 (g/mg.min)	0.030	0.062	0.079	0.049	0.051	0.065	0.008	0.012	0.034	0.012	0.015	0.102
	Δq (%)	0.027	0.017	0.011	0.002	0.002	0.004	0.073	0.030	0.001	0.127	0.003	0.003
	χ^2	0.002	0.001	0.002	0.001	0.001	0.001	0.003	0.005	1.217	0.010	0.001	0.065
	R_2^2	0.994	0.997	0.997	0.972	0.988	0.991	0.922	0.986	1.000	0.956	0.989	0.931

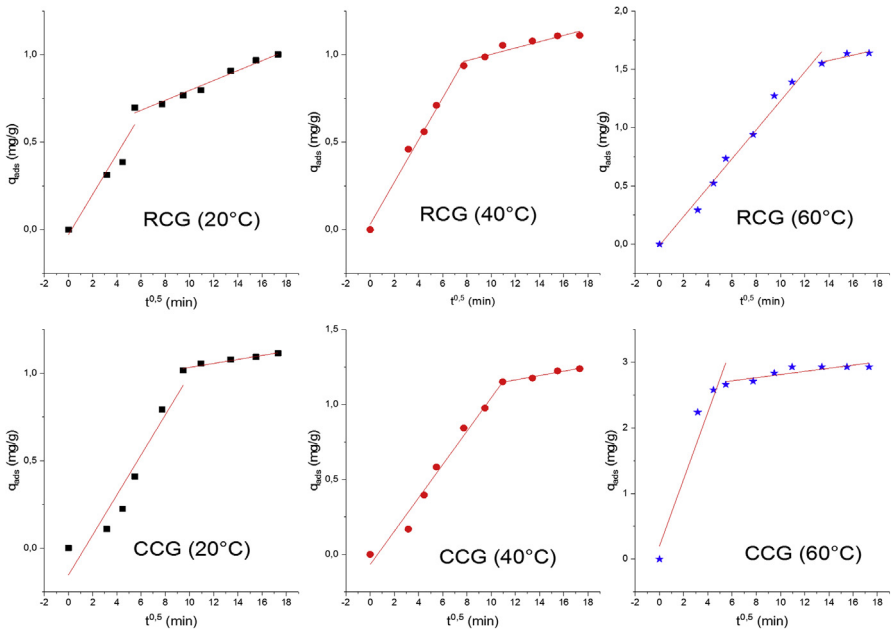

Fig. 7. Intra-particle diffusion model for phenol adsorption onto RCG and CCG.

Table 4
Parameters of the intra-particle diffusion model equations.

Sample	T (°C)	Step 1				Step 2			
		k_{d1} (mg/g).min^{-1}	C_1	R_1^2	SD	k_{d2} (mg/g).min^{-1}	C_2	R_2^2	SD
RCG	20	0.115	−0.028	0.917	0.020	0.028	0.513	0.973	0.002
	40	0.121	0.030	0.991	0.004	0.018	0.822	0.893	0.003
	60	0.124	−0.010	0.983	0.037	0.023	1.249	0.808	0.001
CCG	20	0.114	−0.153	0.918	0.066	0.011	0.919	0.955	0.0002
	40	0.111	−0.068	0.979	0.023	0.015	0.989	0.966	0.0002
	60	0.509	0.199	0.928	0.342	0.024	2.575	0.764	0.019

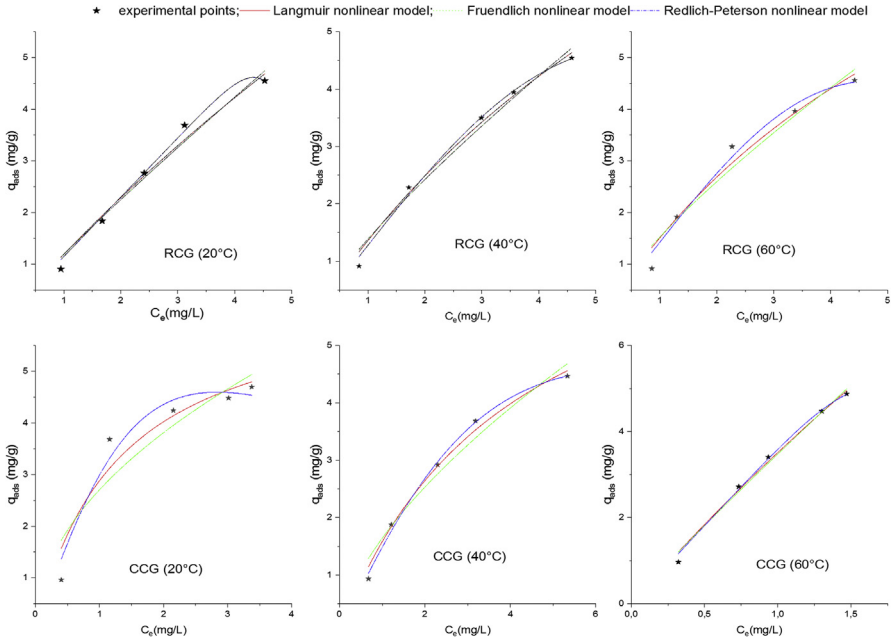

Fig. 8. Adsorption isotherms of the phenol onto RCG and CCG at different temperatures with non-linear fit of Langmuir, Freundlich and Redlich-Peterson models.

Table 5
Model parameters for the adsorption of phenol on RCG and CCG at different temperatures.

	Sample	RCG			CCG		
Model	T (°C)	20	40	60	20	40	60
Langmuir	q_m (mg/g)	27.426	14.065	12.109	6.652	8.054	37.585
	K_L (L/mg)	0.045	0.107	0.142	0.764	0.245	0.103
	R^2	0.981	0.989	0.968	0.922	0.990	0.992
	χ^2	0.054	0.030	0.094	0.244	0.027	0.026
Freundlich	K_F (mg/g)	1.193	1.387	1.525	2.706	3.141	3.478
	1/n	0.914	0.804	0.767	0.494	0.626	0.936
	R^2	0.976	0.980	0.952	0.854	0.964	0.989
	χ^2	0.068	0.056	0.142	0.457	0.095	0.034
Redlich-Peterson	$K_{P\text{-}R}$	1.231E-10	0.005	0.005	0.163	0.048	0.011
	A	1.148	1.286	1.431	3.476	1.553	3.627
	β	13.822	2.662	2.942	1.872	1.724	5.583
	R^2	0.994	0.995	0.982	0.959	0.997	0.995
	χ^2	0.027	0.005	0.005	0.190	0.012	0.023

the adsorption (kJ/mol).

By plotting Ln (k_2) versus 1/T (the Figure is not shown) the slopes lead to Ea values for phenol adsorption onto RCG and CCG, which are 19 kJ.mol^{-1} and 42 kJ.mol^{-1}, respectively. The activation energy range is less than 50 kJ/mol, suggesting a physisorption mechanism. Indeed, when the rate is controlled by the film diffusion mechanism, the activation energy is very low (less than 40 kJ/mol).

3.5. Adsorption isotherms

Phenol adsorption isotherm experiments on both RCG and CCG solids were studied in the initial concentration range of 10–50 mg/L. The obtained experimental points have been represented given in Fig. 8, which represents the evolution of the adsorbed quantity of the phenol versus the residual concentration at different temperatures (20–60 °C). Similarly of kinetic studies, non-linear forms of the Langmuir, Freundlich and Redlich-Peterson (R–P) models were used to analyse the effect of initial concentration. Fig. 8 shows the nonlinear curves of these models at different temperatures and the parameter values derived from these models are presented in Table 5. In addition, to determine the most suitable model to describe the adsorption isotherms of phenol on both solids the nonlinear modelling has been performed. Comparing the values of R^2 and χ^2 (Table 5) we find that the nonlinear Freundlich and Redlich-Peterson models better describe the results of the phenol

Table 6
Thermodynamic parameters for adsorption of phenol onto RCG and CCG.

	T (°C)	ΔS° (J/K, mol)	ΔH° (kJ/mol)	ΔG° (kJ/mol)	R^2
RCG	20	18.572	4.996	−0.445	0.991
	40			−0.817	
	60			−1.188	
CCG	20	25.734	5.103	−2.437	0.995
	40			−2.951	
	60			−3.466	

adsorption isotherm ($R^2 > 0.98$). Indeed, the Langmuir model supposes the formation of a monolayer of the adsorbed quantity of the adsorbate on homogeneous sites of the adsorbent, which is not the case in this study. In addition, it was known that the R–P model is a combination of Langmuir and Freundlich models and that, therefore, the phenol adsorption mechanism on both adsorbents must depend on the β values, which characterize the homogeneity or the heterogeneity of the adsorption sites [53, 54]. Kupeta et al. [53] found that the adsorption of 2-nitrophenol on the raw pine better followed the Freundlich isotherm for β between 0.85 and 0.96, and suggested the formation of a mixture of monolayers and multilayers on the adsorbent. According to the curve of the isotherms, it appears that the Freundlich model is the most suitable for describing the adsorption of phenol on the two adsorbents at the temperature and concentration ranges studied. Indeed, the K_F values increase and the parameter 1/n is less than unity, which indicates that the adsorption affinity of the two solids is favourable towards the phenol.

3.6. Thermodynamic study

Standard thermodynamic parameters such as enthalpy (ΔH°), entropy (ΔS°) and Gibbs free energy (ΔG°) for phenol adsorption onto RCG and CCG were determined using the following relationships:

$$\ln K_F = -\frac{\Delta H^\circ}{RT} + \frac{\Delta S^\circ}{R} \tag{11}$$

$$\Delta G^\circ = \Delta H^\circ - T\Delta S^\circ \tag{12}$$

Where R (8.314 J/K.mol) is the gas constant, K_F (L/mg) is the Freundlich isothermal constant and T (K) is the temperature of the solution.

The plot of Ln (K_F) versus 1/T (the Figure is not shown) leads to the straight lines whose slope is ΔH°. Table 6 summarizes the values of ΔH°, ΔS° and ΔG°. The positive values of ΔH° and ΔS° respectively indicate the endothermic nature which corresponds to the adsorption isotherm and an increase of random character of the phenol molecules at the solid-liquid interfaces, respectively. The values of ΔH° (<40 kJ/mol) indicate that adsorption of phenol on both solids is of a physical nature, confirming the values found for activation energies, implying low attraction between phenol and surface of adsorbents; while those of ΔS° show that the phenol molecules were more ordered on RCG than on CCG. The negative values of ΔG° indicate the spontaneous nature of the adsorption of phenol, and that its adsorption is more favorable at the high temperatures on the two solids.

3.7. Mechanism study

3.7.1. FTIR

The FTIR spectra of RCG and GCC before and after adsorption of phenol are given in Fig. 9. The characteristic bands of RCG and GCC appearing at 3625, 3420 cm^{-1} are attributed to the internal OH units of the kaolinite structure and to the water of hydration of the sodium cation [55]. For RCG and CCG bands (3400–3650 cm^{-1}), there is an increase in intensity as the phenol concentration increases. These results suggest that phenol penetrates the intermediate layer of kaolinite and that the phenol is adsorbed by hydrogen bonding to the water molecules contained in the sphere of hydration of the cations.

In Fig. 9a, for Ph (10^{-3}M)/RCG, the CH band located at 1450 cm^{-1} is resolved in tow peaks. While, in Fig. 9b for the same concentration, the band of CH presents only a single peak with the increasing of intensity. These changes are caused by the deformation vibration in the plane of the phenol CH group. The separation of the bands is also observed for the vibrations below 1030 cm^{-1}, which correspond to the Si–O deformation and Si–O–Si elongation vibrations, which means their involvement in phenol interactions [56].

3.7.2. XRD

The spectra of RCG and CCG are plotted in Fig. 10. The spectra of the RCG indicate the disappearance of the quartz line at 20° in the spectrum of the RCG after adsorption of the phenol, which means in the XRD analysis an exfoliation of the interfoliar space of the solid, which is in this case due to the

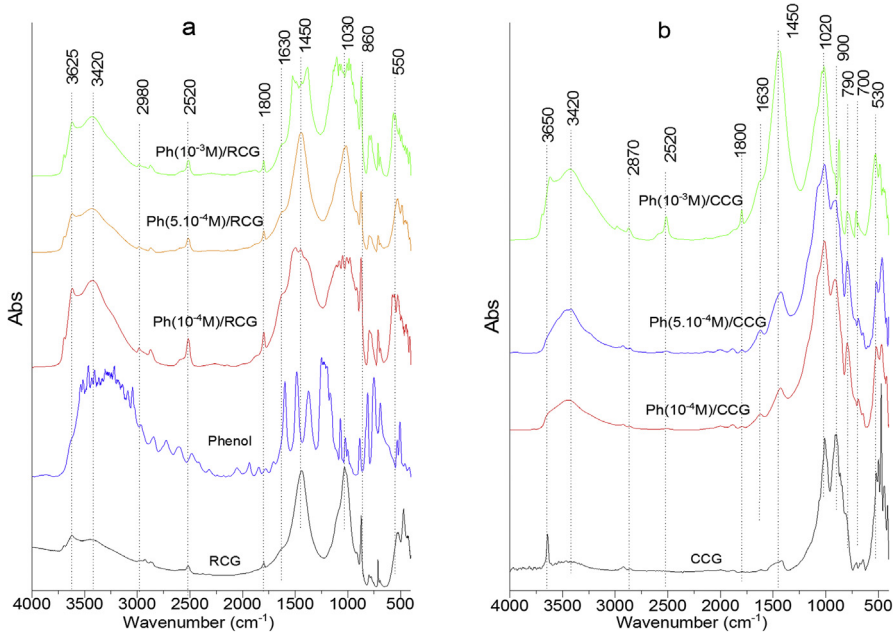

Fig. 9. FTIR spectra of RCG (a) and CCG (b) before and after adsorption of phenol.

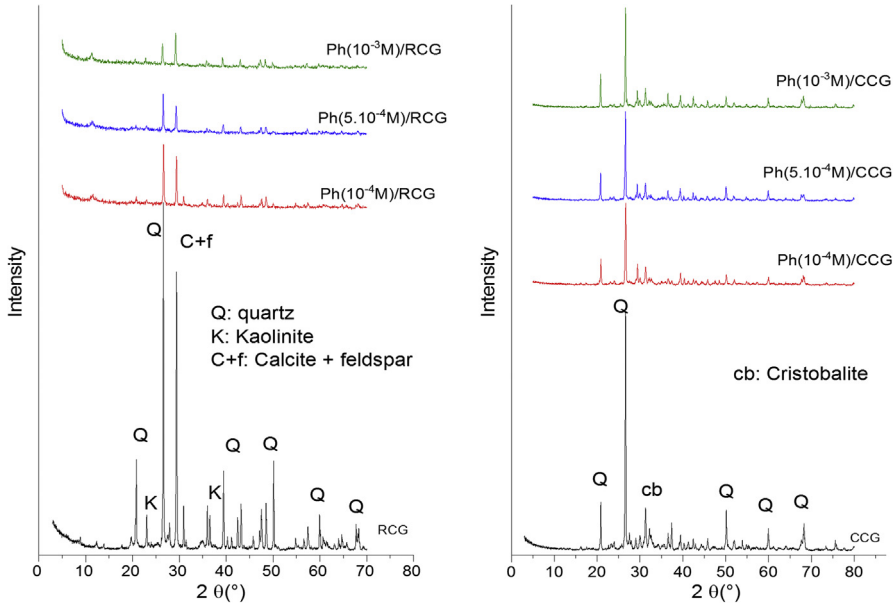

Fig. 10. XRD patterns of RCG and CCG before and after adsorption of phenol.

insertion of the phenol in this space at a large angle of inclination [57]. Indeed, the average diameter of the phenol molecule is 5 Å, and, according to the mode of its penetration into the interfoliar space, the distance of the quartz plane can only increase if this adsorption mechanism [27] is admitted. Also, there is a decrease in peak intensities in the RCG spectra after adsorption of phenol. For those of CCG after adsorption of phenol in finding that there is a decrease in spectral intensities after adsorption of phenol without disappearance of the quartz line. This is explained by the fact that the calcination of the clay increased its interfoliar space (B.E.T result) therefore the concentration of the phenol used was not sufficient to exfoliate the interfoliar space of CCG unlike RCG. Indeed, no new appeared peak in the spectra of the two solids after adsorption of phenol which confirms the physisorption of phenol as previously found.

4. Conclusion

The physicochemical characterization made it possible to highlight the chemical composition of RCG as well as the phyllite and mineral phases present in the two solids. We have also established that the specific surface area of the clay increases from 25.35 m^2/g to 62.21 m^2/g after calcination and that the diameter increases from 38.36 Å to 53.25 Å. This indicates a meso porous structure and that the calcination removes organic matter in the interfoliar spaces.

The adsorption tests show that the used clays have a high capacity to remove phenol. The adsorption is very fast with a contact time not exceeding 3 h and the amount adsorbed increases with temperature. The CCG is more effective than the RCG. Thus, the kinetic result of the adsorption of phenol on the clay materials is followed by the pseudo-second order model and the isotherm is described by the Freundlich and R–P models. The value of the enthalpy ΔH° is less than 20 kJ/mol and the free energy ΔG° has a negative value, which means that the adsorption is done physically and spontaneously on heterogeneous sites. Finally, it is found that the adsorption mechanism of phenol is provided by the hydrogen bonding of the water molecules.

Declarations

Author contribution statement

Hassan Ouallal: Conceived and designed the experiments; Performed the experiments.

Younes Dehmani: Performed the experiments.

Hamou Moussout: Analyzed and interpreted the data; Wrote the paper.

Lahcen Messaoudi, Mohamed Azrour: Contributed reagents, materials, analysis tools or data.

Funding statement

This research did not receive any specific grant from funding agencies in the public, commercial, or not-for-profit sectors.

Competing interest statement

The authors declare no conflict of interest.

Additional information

No additional information is available for this paper.

References

[1] M. Ahmaruzzaman, Adsorption of phenolic compounds on low-cost adsorbents: a review, Adv. Colloid Interface Sci. 143 (2008) 48–67.
[2] M. Moradi, A.M. Mansouri, N. Azizi, J. Amini, K. Karimi, K. Sharafi, Adsorptive removal of phenol from aqueous solutions by copper (cu)-modified scoria powder: process modeling and kinetic evaluation, Desalination Water Treat. 57 (2016) 11820–11834.
[3] K. Sharafi, M. Pirsaheb, V.K. Gupta, S. Agarwal, M. Moradi, Y. Vasseghian, E.N. Dragoi, Phenol adsorption on scoria stone as adsorbent – application of response surface method and artificial neural networks, J. Mol. Liq. 274 (2019) 699–714.
[4] G. Busca, S. Berardinelli, C. Resini, L. Arrighi, Technologies for the removal of phenol from fluid streams: a short review of recent developments, J. Hazard. Mater. 160 (2008) 265–288.
[5] C. Yang, Y. Qian, L. Zhang, J. Feng, Solvent extraction process development and on-site trial-plant for phenol removal from industrial coal-gasification wastewater, Chem. Eng. J. 117 (2006) 179–185.
[6] N. El Hannafi, M.A. Boumakhla, T. Berrama, Z. Bendjama, Elimination of phenol by adsorption on activated carbon prepared from the peach cores: modelling and optimisation, Desalination 223 (2008) 264–268.
[7] G. Hublik, F. Schinner, Characterization and immobilization of the laccase from Pleurotus ostreatus and its use for the continuous elimination of phenolic pollutants, Enzyme Microb. Technol. 27 (2000) 330–336.
[8] H. Saito, K. Miura, Preparation of transforming deoxyribonucleic acid by phenol treatment, Biochim. Biophys. Acta 72 (1963) 619–629.
[9] C. Catrinescu, C. Teodosiu, M. Macoveanu, J. Miehe-Brendlé, R. Le Dred, Catalytic wet peroxide oxidation of phenol over Fe-exchanged pillared beidellite, Water Res. 37 (2003) 1154–1160.

[10] Z. Aksu, D. Akpinar, Simultaneous adsorption of phenol and chromium (VI) from binary mixtures onto powdered activated carbon, J. Environ. Sci. Heal. Part A Toxic Hazard. Subst. Environ. Eng. 35 (2000) 379–405.
[11] G. Annadurai, R.-S. Juang, D.-J. Lee, Biodegradation and adsorption of phenol using activated carbon immobilized with *Pseudomonas putida*, J. Environ. Sci. Heal. Part A 37 (2002) 1133–1146.
[12] N.S. Abuzeid, I.M. Harrazin, Effect of CO_2 on the adsorption of phenol and o-cresol on granular activated carbon, J. Environ. Sci. Heal. Part A Environ. Sci. Eng. Toxicol. 26 (1991) 257–271.
[13] F.C. Wu, R.L. Tseng, R.S. Juang, Preparation of activated carbons from bamboo and their adsorption abilities for dyes and phenol, J. Environ. Sci. Heal. Part A Toxic Hazard. Subst. Environ. Eng. 34 (1999) 1753–1775.
[14] M.S.E. Abdo, S.A. Nosier, Y.A. ElTawil, S.M. Fadl, M.I. ElKhaiary, Removal of phenol from aqueous solutions by mixed adsorbents: Maghara coal and activated carbon, J. Environ. Sci. Heal. 32 (1997) 1159–1169.
[15] H. Sadki, K. Ziat, M. Saidi, Adsorption of dyes on activated local clay in aqueous solution, J. Mater. Environ. Sci. 5 (2014) 2060–2065.
[16] E.G. Garrido-Ramírez, B.K.G. Theng, M.L. Mora, Clays and oxide minerals as catalysts and nanocatalysts in Fenton-like reactions – a review, Appl. Clay Sci. 47 (2010) 182–192.
[17] S.H. Lin, R.S. Juang, Adsorption of phenol and its derivatives from water using synthetic resins and low-cost natural adsorbents: a review, J. Environ. Manage. 90 (2009) 1336–1349.
[18] S.M. Lee, T.W. Lee, B.J. Choi, J.K. Yang, Treatment of Cr(VI) and phenol by illuminated TiO_2, J. Environ. Sci. Heal. Part A Toxic Hazard. Subst. Environ. Eng. 38 (2003) 2219–2228.
[19] P.X. Wu, Z.W. Liao, H.F. Zhang, J.G. Guo, Adsorption of phenol on inorganic-organic pillared montmorillonite in polluted water, Environ. Int. 26 (2001) 401–407.
[20] A.E.S. Choi, S. Roces, N. Dugos, M.W. Wan, Adsorption of benzothiophene sulfone over clay mineral adsorbents in the frame of oxidative desulfurization, Fuel 205 (2017) 153–160.
[21] Q. Xiu Jing, L. Yuan Chai, X. Dong Huang, C. Jian Tang, H. Guo, W. Wang, Behavior of ammonium adsorption by clay mineral halloysite, Trans. Nonferrous Met. Soc. China Engl. Ed. 27 (2017) 1627–1635.
[22] H. Moussout, H. Ahlafi, M. Aazza, O. Zegaoui, C. El Akili, Adsorption studies of Cu(II) onto biopolymer chitosan and its nanocomposite 5% bentonite/chitosan, Water Sci. Technol. 73 (2016) 2199–2210.
[23] H. Moussout, H. Ahlafi, M. Aazza, C. El Akili, Performances of local chitosan and its nanocomposite 5%Bentonite/Chitosan in the removal of chromium ions (Cr(VI)) from wastewater, Int. J. Biol. Macromol. 108 (2018) 1063–1073.
[24] L. Ma, J. Zhu, Y. Xi, R. Zhu, H. He, X. Liang, G.A. Ayoko, Adsorption of phenol, phosphate and Cd(II) by inorganic-organic montmorillonites: a comparative study of single and multiple solute, Colloids Surf. A Physicochem. Eng. Asp. 497 (2016) 63–71.
[25] A.M. Georgescu, F. Nardou, V. Zichil, I.D. Nistor, Adsorption of lead(II) ions from aqueous solutions onto Cr-pillared clays, Appl. Clay Sci. 152 (2018) 44–50.
[26] A. Gładysz-Płaska, M. Majdan, S. Pikus, D. Sternik, Simultaneous adsorption of chromium(VI) and phenol on natural red clay modified by HDTMA, Chem. Eng. J. 179 (2012) 140–150.
[27] S. Richards, A. Bouazza, Phenol adsorption in organo-modified basaltic clay and bentonite, Appl. Clay Sci. 37 (2007) 133–142.
[28] Y. Li, X. Hu, X. Liu, Y. Zhang, Q. Zhao, P. Ning, S. Tian, Adsorption behavior of phenol by reversible surfactant-modified montmorillonite: mechanism, thermodynamics, and regeneration, Chem. Eng. J. 334 (2018) 1214–1221.
[29] M.H. Al-Malack, M. Dauda, Competitive adsorption of cadmium and phenol on activated carbon produced from municipal sludge, J. Environ. Chem. Eng. 5 (2017) 2718–2729.
[30] Z. Luo, M. Gao, S. Yang, Q. Yang, Adsorption of phenols on reduced-charge montmorillonites modified by bispyridinium dibromides: mechanism, kinetics and thermodynamics studies, Colloids Surf. A Physicochem. Eng. Asp. 482 (2015) 222–230.
[31] M.K. Uddin, A review on the adsorption of heavy metals by clay minerals, with special focus on the past decade, Chem. Eng. J. 308 (2017) 438–462.
[32] M. Aazza, H. Ahlafi, H. Moussout, H. Maghat, Ortho-nitro-phenol adsorption onto alumina and surfactant modified alumina: kinetic, isotherm and mechanism, J. Environ. Chem. Eng. 5 (2017) 3418–3428.
[33] J. Lesur, E.A. Hildebrand, G. Abawa, X. Gutherz, The advent of herding in the Horn of Africa: new data from Ethiopia, Djibouti and Somaliland, Quat. Int. 343 (2014) 148–158.
[34] O. Abdelwahab, N.K. Amin, Adsorption of phenol from aqueous solutions by *Luffa cylindrica* fibers: kinetics, isotherm and thermodynamic studies, Egypt, J. Aquat. Res. 39 (2013) 215–223.
[35] R. San Nicolas, M. Cyr, G. Escadeillas, Characteristics and applications of flash metakaolins, Appl. Clay Sci. 83–84 (2013) 253–262.
[36] V. Zaspalis, A. Pagana, S. Sklari, Arsenic removal from contaminated water by iron oxide sorbents and porous ceramic membranes, Desalination 217 (2007) 167–180.
[37] T. Sheela, Y.A. Nayaka, Kinetics and thermodynamics of cadmium and lead ions adsorption on NiO nanoparticles, Chem. Eng. J. 191 (2012) 123–131.
[38] D. Hank, Z. Azi, S. Ait Hocine, O. Chaalal, A. Hellal, Optimization of phenol adsorption onto bentonite by factorial design methodology, J. Ind. Eng. Chem. 20 (2014) 2256–2263.
[39] J.R.O. Kikouama, K.L. Konan, A. Katty, J.P. Bonnet, L. Baldé, N. Yagoubi, Physicochemical characterization of edible clays and release of trace elements, Appl. Clay Sci. 43 (2009) 135–141.
[40] P. Sabbatini, F. Rossi, G. Thern, A. Marajofsky, M.M.F. de Cortalezzi, Iron oxide adsorbers for arsenic removal: a low cost treatment for rural areas and mobile applications, Desalination 248 (2009) 184–192.
[41] K.P. Raven, A. Jain, R.H. Loeppert, Arsenite and arsenate adsorption on ferrihydrite: kinetics, equilibrium, and adsorption envelopes, Environ. Sci. Technol. 32 (1998) 344–349.
[42] J. Ojima, Determining of crystalline silica in respirable dust samples by infrared spectrophotometry in the presence of interferences, J. Occup. Health 45 (2003) 94–103.
[43] R. Fernandez, F. Martirena, K.L. Scrivener, The origin of the pozzolanic activity of calcined clay minerals: a comparison between kaolinite, illite and montmorillonite, Cem. Concr. Res. 41 (2011) 113–122.
[44] R. Mejía de Gutiérrez, J. Torres, C. Vizcayno, R. Castello, Influence of the calcination temperature of kaolin on the mechanical properties of mortars and concretes containing metakaolin, Clay Miner. 43 (2008) 177–183.
[45] F. Bergaya, The meaning of surface area and porosity measurements of clays and pillared clays, J. Porous Mater. 2 (1995) 91–96.
[46] J.T. Kloprogge, Synthesis of smectites and porous pillared clay catalysts: a review, J. Porous Mater. 5 (1998) 5–41.
[47] P.G. Weidler, BET sample pretreatment of synthetic ferrihydrite and its influence on the determination of surface area and porosity, J. Porous Mater. 4 (1997) 165–169.
[48] J.Q. Jiang, S.M. Ashekuzzaman, J.S.J. Hargreaves, A.R. Mcfarlane, A.B.M. Badruzzaman, M.H. Tarek, Removal of arsenic (III) from groundwater applying a reusable Mg-Fe-Cl layered double hydroxide, J. Chem. Technol. Biotechnol. 90 (2015) 1160–1166.
[49] D. Karadag, E. Akgul, S. Tok, F. Erturk, M.A. Kaya, M. Turan, Basic and reactive dye removal using natural and modified zeolites, J. Chem. Eng. Data 52 (2007) 2436–2441.
[50] P.S. Nayak, B.K. Singh, Sorption studies on clay for the removal of phenol and p-nitrophenol from aqueous solution, Indian J. Chem. Sect. A Inorg. Phys. Theor. Anal. Chem. 46 (2007) 620–623.
[51] H.N. Tran, S.J. You, A. Hosseini-Bandegharaei, H.P. Chao, Mistakes and inconsistencies regarding adsorption of contaminants from aqueous solutions: a critical review, Water Res. 120 (2017) 88–116.
[52] H. Moussout, H. Ahlafi, M. Aazza, H. Maghat, Critical of linear and nonlinear equations of pseudo-first order and pseudo-second order kinetic models, Karbala Int. J. Mod. Sci. 4 (2018) 244–254.
[53] A.J.K. Kupeta, E.B. Naidoo, A.E. Ofomaja, Kinetics and equilibrium study of 2-nitrophenol adsorption onto polyurethane cross-linked pine cone biomass, J. Clean. Prod. 179 (2018) 191–209.
[54] F. Haghseresht, G.Q. Lu, Adsorption characteristics of phenolic compounds onto coal-reject-derived adsorbents, Energy Fuels 12 (1998) 1100–1107.
[55] J. Madejova, FTIR techniques in clay mineral studies, Vib. Spectrosc. 31 (2003) 31.
[56] A. Tabak, B. Afsin, S.F. Aygun, E. Koksal, Structural characteristics of organo-modified bentonites of different origin, J. Thermal Anal. Calorim. 87 (2007) 375–381.
[57] R. Liu, R.L. Frost, W.N. Martens, Near infrared and mid infrared investigations of adsorbed phenol on HDTMAB organoclays, Mater. Chem. Phys. 113 (2009) 707–713.